CONSEQUENCES OF SHALLOW LUNAR MAGMATIC INTRUSION: VENTING, PYROCLASTICS, AND SUBSIDENCE ASSOCIATED WITH FLOOR-FRACTURED CRATERS. L. M. Jozwiak[1], J. W. Head[1], and L. Wilson[2], [1]Department of Geological Sciences, Brown University, 324 Brook St, Providence, RI 02912. (lauren_jozwiak@brown.edu), [2] Lancaster Environment Centre, Lancaster University, Lancaster LA1 4YQ UK

Introduction: Floor-fractured craters are a class of lunar crater characterized by anomalously shallow, fractured floors, with additional characteristics including moats, dark halo deposits, and patches of mare material [1,2]. The two proposed formation mechanisms for floor-fractured craters are 1) viscous relaxation [1,3] and magmatic intrusion and sill emplacement [1]. Recent morphologic analysis using Lunar Orbiter and Laser Altimeter (LOLA) and Lunar Reconnaissance Orbiter Camera (LROC) data and images supports magmatic intrusion and sill emplacement as the formation mechanism of floor-fractured craters [2].

Exploring this interpretation, we examine the consequences of a large, shallow magmatic body beneath a lunar crater. Specifically, we investigate the processes associated with degassing and cooling of the magma body and the subsequent possibilities of venting, pyroclastic eruptions, and subsidence. We use the expected morphologic effects of these processes to further assess the formation of floor-fractured craters by magmatic intrusion.

Magma Degassing: In the magmatic intrusion hypothesis, magma is intruded beneath a crater at a depth of one to a few kilometers below the surface, with this depth being derived from the postulated intrusion dimensions [2,4]. The postulated intrusion dimensions are derived from LOLA topographic data. The intrusion diameter represents the uplifted region of the crater floor, and the intrusion thickness is the difference between the observed crater depth and the typical depth of a fresh crater of the same diameter [5]. During magma ascent, reactions between free carbon and metal oxides produce CO, which rises as a gas+magmatic foam layer to the top of the dike, and later sill [6,7,8]. To determine the potential volume of this foam layer, we assume a gas concentration of 1000 ppm in the initial magma [6,8,9], and a gas mass fraction, *n*, that is dependent on the excess pressure needed to fracture the overlying rock [9]. Then, using the current intrusion volume, we calculate the initial volume of the foam rich layer [9].

We take the crater Gassendi (Figure 1a) as an archetypal example of a large, Class 3 floor-fractured crater [2]. Using the LOLA derived intrusion dimensions radius ~48 km and intrusion thickness ~2 km [2], an unvesiculated lunar magma density of 3000 kg/m^3, and assuming that all of the CO scavenged from the intrusion magma resides in the upper foam layer, we calculate a mass of CO ~$2*10^{10}$ kg. We assume a pressure of ~15 MPa, which is approximately twice the tensile strength of basalt [9, 10, 11]. This value is also a valid approximation for a ceiling rock composed of igneous basalt, which has demonstrated a similar failure stress criterion to igneous basalts in uniaxial compression tests [12]. We then take *n* ~0.0239 for the foam layer which corresponds to the 15 MPa pressure [9], calculate the mass of magma in the foam layer, sum the masses and divide by the density of foam layer, β~924 kg/m^3 [9] to find a total foam layer volume of ~$10*10^8$ m^3.

Pyroclastic Eruptions: One of the most important consequences of magma reservoir degassing is the relief of the additional pressure, either by passive venting along pre-formed fractures or by pyroclastic eruptions.

The floor-fractured crater Alphonsus hosts several dark halo craters which are hypothesized to be the result of vulcanian or ultra-vulcanian eruptions [13], implying crustal fracture by volatile-rich foam, as would be the scenario for a feature in a floor-fractured crater with a large body of magma beneath it. The dark halo craters in Alphonsus (Figure 2) are located primarily along the floor-fractures, suggesting a relationship between the two processes. *Head and Wilson* [1979] suggest a case wherein magma partially fills a fracture before solidifying, a foam-rich layer then builds beneath this cap, and when the critical pressure is reached, a vulcanian eruption takes place (Figure 3). Given such a formation mechanism, there should be a strong correlation between floor-fractured craters formed by magmatic intrusion, and observed venting features, such as dark halo craters, along the floor-fractures.

By calculating the volume of the volatile-rich foam layer for various intrusion sizes, we can predict which floor-fractured craters are likely to experience pyroclastic eruptions, and then compare these with observed pyroclastic deposits and vents, such as the dark halo craters in Alphonsus and Schrödinger.

Subsidence and Fracturing: Subsidence is another key aspect of the degassing of a magma reservoir. In terrestrial eruptive cycles, subsidence is regularly observed prior to, and coincident with, magma degassing events, such as steam plumes observed at Lascar Volcano in Chile [14]. The formation and reinforcement of concentric fractures surrounding the subsided dome is also noted [14]. *Marti et. al.* [1994] performed laboratory analog experiments recording the fracture styles associated with periods of inflation and subsidence [15]. The experiments indicated that shallow polygonal fractures and radial fractures formed predominately during doming, and that concentric fractures formed predominately during

subsidence, although concentric fractures could also form during the doming stage [15].

These three fracture styles—polygonal, radial, and concentric—are all observed in floor-fractured craters [1,2], with different morphologic classes showing preference for different styles of floor-fracturing. Examples of these polygonal and concentric floor-fractures from crater Gassendi are shown in Figure 1a.

By analyzing the observed fracture patterns as they relate to the morphologic classes of floor-fractured craters [2], and using LOLA generated topographic floor profiles, we examine the cycles of uplift and potential subsidence that occurred. For example, in Gassendi, initial uplift of the crater floor produced the polygonal fractures observed throughout the crater. Additionally, there is a concentric fracture in the northwestern part of the crater; this area appears to have subsided relative to the southeastern portion of the crater floor (Figure 1b). The theoretical subsidence caused by the total removal of the foam layer beneath Gassendi is ~13m; however, this assumes equal distribution of the foam across the area of the intrusion. If we postulate that the foam collected preferentially in the area of highest elevation, thus lowest lithostatic pressure, the subsidence becomes ~25 m in the northern part of the crater, similar to that observed in Figure 1b. These analyses are then cumulatively combined with the analytic calculations of pyroclastic potential and the morphologic evidence for pyroclastic deposits and vents to further investigate the strong case for floor-fractured crater formation via magmatic intrusion and sill formation.

Conclusions: We explore the hypothesis that floor-fractured craters are formed by magmatic intrusion and sill formation, as has been suggested by recent interpretations of morphologic data [2], by examining the process of magma degassing in such a reservoir, and the subsequent nature of pyroclastic eruptions and floor subsidence. As an example, we calculate the thickness of the foam layer beneath the crater Gassendi, based on the LOLA topography derived intrusion dimensions [2]. Assuming the foam collects preferentially in the higher elevations of the crater floor, the amount of subsidence resulting from the removal of this foam layer corresponds closely to the observed topographic difference between the northwestern section of the floor of Gassendi compared with the domed southern section (Figure 1b). The polygonal fractures on the floor of Gassendi are interpreted to correspond to uplift-induced fractures [15], and the concentric fractures in the northwestern part of the crater to the topographically subsided region.

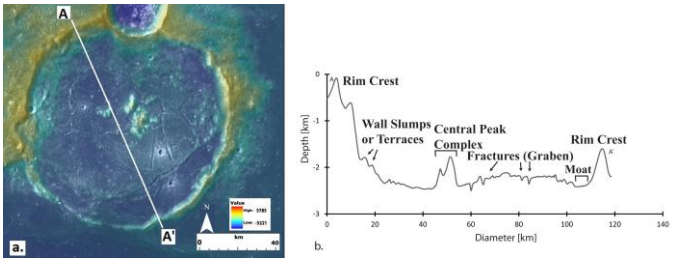

Figure 1: LOLA topography with overlaid LROC-WAC imagery depicting the crater Gassendi. Figure 1a shows the series of polygonal and concentric fractures that cross the floor. Figure 1b shows a LOLA topographic profile across the floor of Gassendi, note the uneven uplift which we interpret to be the result of subsidence in certain parts of the crater floor [2].

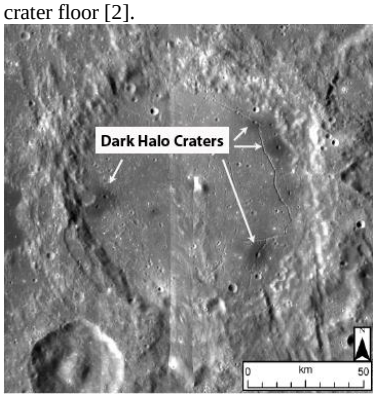

Figure 2: LROC-WAC image depicting the crater Alphonsus. The crater hosts dark halo craters, which comprise a central depression surrounded by dark mantle material.

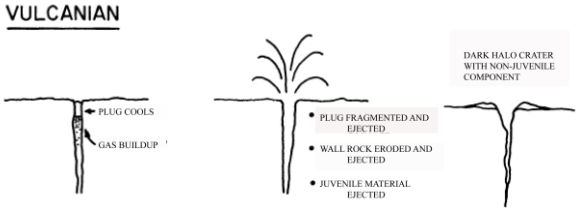

Figure 3: Cross-section of the vulcanian eruption process that formed the observed dark halo craters in crater Alphonsus. Intruded magma initially cools in a fracture. The magma then degasses and when the critical pressure is exceeded, a vulcanian eruption takes place [9].

References: [1] Schultz P. H. (1976) *Moon, 15,* 241-273. [2] Jozwiak L. M. et al. (2012) *JGR., 117,* E11. [3] Hall et. al. (1981) *JGR, 86,* 9537-9552. [4] Wichman R.W. and Schultz P.H. (1996) *Icarus, 122,* 193-199. [5] Pike R.J. (1980) *U.S.G.S. Prof. Paper, 1046-C,* C1-C77. [6] Sato M. (1979) *LPS X,* 311-325. [7] Fogel R. and Rutherford M. (1995) *Geochim. Cosmochim. Acta, 59,* 201-215. [8] Wilson L. and Head J. W. (2003) *GRL, 30:12,* 1650. [9] Head J.W. et. al. (2002) *JGR, 107,* E1. [10] Touloukian et. al. (1980) *Physical Properties Of Rocks and Minerals* [11] Tait S. et. al. (1989) *EPSL, 92,* 107-123. [12] E. Hoek and E.T. Brown (1997) *Int. J. Rock Mech. Min. Sci., 34,* 1165-1186. [13] Head J.W. and Wilson L. (1979) *LPS X,* 2861-2897. [14] Matthews S.J. et. al. (1997) *Bull. Volcanol., 59,* 72-82. [15] Marti J. et. al. (1994) *J. of Geol. Soc. London, 151,* 919-929.